12-2007

Passive Fathometer Processing

Peter Gerstoft
Marine Physical Laboratory

William S. Hodgkiss
Marine Physical Laboratory

Martin Siderius
Portland State University, siderius@pdx.edu

Chen-Fen Huang
Department of Marine Environmental Informatics

Chris H. Harrison
NURC

Citation Details

Gerstoft, P., Hodgkiss, W. S., Siderius, M., Chen-Fen, H., & Harrison, C. H. (2008). Passive fathometer processing. Journal of The Acoustical Society of America, 123(3), 1297-1305.

Passive fathometer processing

Peter Gerstoft and William S. Hodgkiss
Marine Physical Laboratory, Scripps Institution of Oceanography, La Jolla, California 92093-0238

Martin Siderius
HLS Research Inc., 3366 North Torrey Pines Court, Suite 310, La Jolla, California 92037

Chen-Fen Huang
Department of Marine Environmental Informatics, National Taiwan Ocean University, Keelung, Taiwan

Chris H. Harrison
NURC, La Spezia, Italy

(Received 21 September 2007; revised 10 December 2007; accepted 10 December 2007)

Ocean acoustic noise can be processed efficiently to extract Green's function information between two receivers. By using noise array-processing techniques, it has been demonstrated that a passive array can be used as a fathometer [Siderius, *et al.*, J. Acoust. Soc. Am. **120**, 1315–1323 (2006)]. Here, this approach is derived in both frequency and time domains and the output corresponds to the reflection sequence. From this reflection sequence, it is possible to extract seabed layering. In the ocean waveguide, most of the energy is horizontally propagating, whereas the bottom information is contained in the vertically propagating noise. Extracting the seabed information requires a dense array, since the resolution of the bottom layer is about half the array spacing. If velocity sensors are used instead of pressure sensors, the array spacing requirement can be relaxed and simulations show that just one vertical velocity sensor is sufficient.
 [DOI: 10.1121/1.2831930]

PACS number(s): 43.30.Pc, 43.60.Pt [AIT] Pages: 1297–1305

I. INTRODUCTION

In recent years it has been demonstrated that the time domain Green's function between a source and a receiver can be extracted from noise, for reviews see Refs. 1 and 2. The theory for this is now relatively well-developed[3–6] and the approach has been demonstrated in ocean acoustics (including ocean waveguides),[7–10] ultrasound,[3] and seismology.[11–18]

The idea is to cross correlate noise wave fields between two receivers and by time averaging over a sufficiently long time only the propagation paths between the two receivers remain. The theory prescribes that the noise should be isotropic. In an ocean acoustic waveguide, the noise is nonisotropic with most noise originating from the surface; this can be modeled as a sheet of sources located close to the surface.[19] The vertically propagating noise is partially reflected from layers of the seabed and eventually dissipated through attenuation losses. For noise propagating at grazing angles lower than critical, this noise is trapped in the ocean waveguide.

Siderius *et al.*[10] introduced a coherent broadband array processing method for a vertical array that limits the effect of the horizontally propagating noise, this is the so-called passive fathometer method. The method is based on relating the down- and up-going signals on the array and can be implemented in the time or frequency domains. In order to develop this fathometer method into a practical processing approach, a number of issues have to be addressed in detail. Several of these are addressed here:

(1) Theory is developed in both time and frequency domains.
(2) It is established that the wavelet is a sinc function.
(3) Adaptive beamforming is introduced for frequency domain processing and shown to give good results.
(4) The important issue of spatial aliasing is discussed.
(5) It is demonstrated that due to strong presence of horizontally propagating noise, the maximum frequency should not be higher than twice the design frequency for a conventional hydrophone array.
(6) Vertical velocity sensors are not sensitive to the horizontally propagating noise and based on simulations, it is shown that just one sensor is sufficient to resolve the seabed layering.

II. SIMPLE EXAMPLE

A simple example motivates the approach and demonstrates that a vertical array can be used as a fathometer, see Fig. 1. Consider a simple 100-m deep ocean with a square pulse (width 0.01 s, amplitude 1) propagating down, reflected, and then propagating up (amplitude 0.5) and recorded on a 50-m long array with 20 receivers as shown in Fig. 1. The processing[10] calls for stacking the down- and up-going signals, Figs. 1(b) and 1(c). This is done by time delaying and summing at a reference depth, in this case (and all examples here) the ocean surface. Both stacked signals show a main peak, corresponding to the wave propagating with that speed, and a spread out waveform, corresponding to the signature obtained from stacking the opposite propagating wave.

Finally, in Fig. 1(d) we cross correlate the down- and up-going signals. This shows a triangular pulse of width

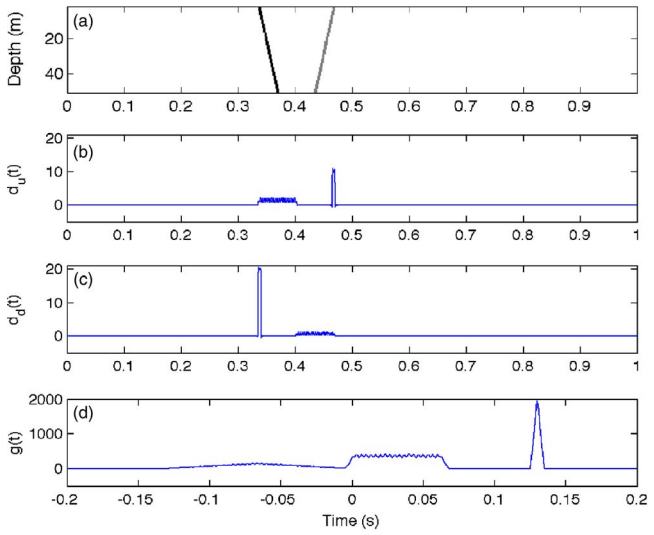

FIG. 1. (Color online) Time domain processing of a simple arrival in a 100-m ocean with 20 receivers at 0–50 m depth. (a) A square pulse 0.1-s wide with a down-going component of amplitude 1 and an up-going component with amplitude 0.5. (b) Stacking the signal at the surface in up-going direction. (c) Stacking the signal at the surface in down-going direction. (d) Cross correlation of the stacked down- and up-going signals.

0.02 s appearing at a travel time corresponding to two water depths ($2\times100/1500=0.13$ s). The triangular shape is due to the convolution of two square pulses. In addition, there is some spurious components visible from about 0 to 0.067 s, due to the convolution of signals that did not propagate in the stacking direction. The time extent of this noise corresponds to twice the travel time across the array length. The corresponding spurious component can be seen in Fig. 1(b) from 0.33 to 0.4 s. Within this interval the level is fairly constant with small variations in amplitude. Though not visible in the plot, the shape at the peaks is a square wave with 19 peaks. The number of small peaks is proportional to the number of hydrophones in the array and depends also on the source wave form.

III. THEORY

First, in Sec. III A a one-dimensional (1D) model is used to demonstrate that the reflection sequence can be extracted by cross correlating the down- and up-going wave fields at a receiver. One way to extract the down- and up-going wave fields is to use beamforming[10] as discussed in the remainder of this section.

The cross-correlation approach can cause spurious components, as demonstrated using interferometric approaches.[9,20,21] A mild example of a spurious component was shown in Fig. 1(d). However, the spurious components can be reduced by cross-correlating down- and up-going wave fields.[22] It is feasible to separate the down- and up-going wavefields by combining the response from a vertical geophone and a hydrophone.[22] Our beamforming approach results in a similar decomposition.

A. 1D model

The environment under consideration is shown in Fig. 2(a). Assuming a simple 1D model, the corresponding block diagram in Fig. 2(b) is obtained, where we cross correlate the down-going signal $d_d(t)$ with the upgoing signal. $d_u(t)$ using a receiver at the surface as a reference. As the noise $w(t)$ is generated near the surface, $d_d(t)=w(t)$. This down-going signal is time delayed by τ corresponding to the travel time to the ocean bottom from the receiver, convolved with the reflection sequence $h(t)$ at the ocean bottom, and time delayed by τ as the signal propagates back to the receiver. This gives ($*$ represents convolution)

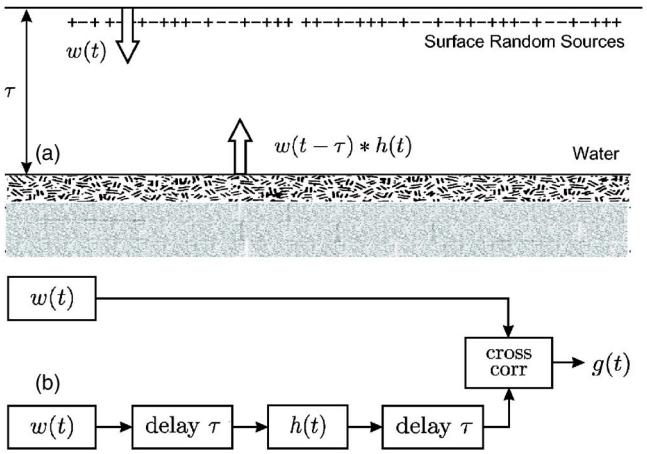

FIG. 2. (Color online) Environment and block diagram. $w(t)$ represents ocean surface noise, $h(t)$ the reflection sequence, and τ the vertical travel time across the ocean.

$$d_u(t) = w(t-2\tau) * h(t). \tag{1}$$

Cross correlating the down- and up-going signals yields

$$c_{ud}(t) = d_u(t) * d_d(-t) = w(t-2\tau) * h(t) * w(-t)$$
$$= [w(t) * w(-t)] * h(t-2\tau). \tag{2}$$

The first term in square brackets is the autocorrelation function of the surface noise time series $w(t)$ (inverse Fourier transform of the surface noise power spectral density function). The last term is the time-delayed seabed reflection sequence, which is related to the Green's function, indicating that by cross correlating the down- and up-going wave fields the seabed reflection sequence and its layering can be extracted. The 2τ term is twice the travel time from the receiver to the ocean floor and this is the idea behind the ocean bottom fathometer,[10] but as indicated in Eq. (2) the whole reflection sequence is available.

Assuming the noise from the sea surface is spectrally flat ("white") then the autocorrelation of a low-pass white noise process with bandwidth b has a sinc($2bt$) wave form.[23] The width of the main peak in the sinc function is $1/b$. Translating this $1/b$ resolution to the two-way travel time to depth gives a depth resolution of about $1/b(c/2)=c/2b$ (c is the sound speed).

Generally the noise cross correlation approach has been successful in estimating travel times, but less successful in obtaining amplitudes. In the literature there appears to be differences in opinion, as it has been suggested that the time domain Green's function is proportional to the noise cross correlation, its time derivative, time integral, or even a fractional derivative. Most current applications are concerned

with obtaining kinematically correct (arrival time) expressions. This does not depend on the time derivative.

Some of this variation in the use of time derivative is related to the dimension of the physical domain in which the wave is propagating and the effective dimension of the source distribution. For example, using a three-dimensional (3D) physical domain and a 1D source as in Refs. 7, 20, and 21 results in a fractional time derivative (a factor $1/\sqrt{i\omega}$ in the frequency domain).

Consider a uniform 1D medium with speed c and a point source [zero-dimensional (0D)] at $z=0$, then the time domain Green's function $g_1(t)$ at distance z would be

$$g_1(t) = \delta\left(t - \frac{z}{c}\right). \tag{3}$$

The cross correlation in the frequency domain between the downward propagating noise at receivers z_1 and z_2 then would be

$$C_{12}(\omega) = e^{i(\omega/c)(z_2 - z_1)}. \tag{4}$$

In the time domain,

$$c_{12}(t) = \delta(t - (z_2 - z_1)/c) = g_1(t). \tag{5}$$

Thus, for a 1D medium with a single point source the Green's function is proportional to the noise cross correlation. As the fathometer closely resembles a 1D medium, this assumption was used in Ref. 10 and is used here as well.

B. Time domain stacking

Extracting the reflection sequence from noise recordings for a vertical array with N sensors at depth z_i is developed in the time domain $p_i(t)$ in this section and in the frequency domain $p_i(\omega)$ in Sec. III C. The Fourier transform pair is given by

$$p(\omega) = \int p(t) e^{-i\omega t} dt, \tag{6}$$

$$p(t) = \frac{1}{2\pi} \int p(\omega) e^{i\omega t} d\omega. \tag{7}$$

The factor $1/2\pi$ is suppressed in the following. Assuming vertical propagation, the time t is converted to depth by dividing by $2c$, where c is a representative speed.

Stacking or summing over the z-coordinate with a time delay corresponding to a slowness $+s=1/c$ for downgoing waves, gives

$$d_d(t) = \sum_{i=1}^{N} p_i(t + s(z_i - z_0)), \tag{8}$$

where the time series are projected into the time series corresponding to depth z_0. We prefer to use slowness because the processing is linear with slowness. Stacking for upgoing waves using the negative slowness $-s$ gives

$$d_u(t) = \sum_{i=1}^{N} p_i(t - s(z_i - z_0)). \tag{9}$$

In the frequency domain the down- and up-going waves can be expressed as

$$d_d(\omega) = \int \sum_{i=1}^{N} p_i(t + s(z_i - z_0)) e^{-i\omega t} dt$$

$$= \sum_{i=1}^{N} p_i(\omega) e^{+i\omega s(z_i - z_0)}, \tag{10}$$

$$d_u(\omega) = \int \sum_{i=1}^{N} p_i(t - s(z_i - z_0)) e^{-i\omega t} dt$$

$$= \sum_{i=1}^{N} p_i(\omega) e^{-i\omega s(z_i - z_0)}. \tag{11}$$

Cross correlation between down- and up-going waves is computed for the whole observation period T

$$c_{ud}(t) = d_u(t) * d_d(-t) = \int_0^T d_u(\tau) d_d(\tau - t) d\tau, \tag{12}$$

where the $1/T$ normalizing factor is neglected. As we are concerned with comparing signals from the top of the ocean with reflected signals from the bottom, the averaging time T should be much larger than twice the travel time over the ocean depth. In the frequency domain Eq. (12) becomes

$$C_{ud}(\omega) = d_u(\omega) d_d^*(\omega). \tag{13}$$

Inverse Fourier transforming $C_{ud}(\omega)$ to the time domain give, $c_{ud}(t)$, which is the reflection sequence convolved with the noise autocorrelation function, see Eq. (2). From this the seabed layering can be estimated.

C. Frequency domain beamforming

By beamforming we can obtain the down- and up-going beams corresponding to down and up-going wave fields, respectively:

$$d_d(\omega) = \mathbf{w}_d^H \mathbf{p}, \tag{14}$$

$$d_u(\omega) = \mathbf{w}_u^H \mathbf{p}, \tag{15}$$

where $\mathbf{p}(\omega) = [p_1(\omega), p_2(\omega, \ldots]^T$ where superscripts T, H, and the asterisk refer to the transpose, complex conjugate transpose, and complex conjugate operators, respectively. $\mathbf{w}_d$ and $\mathbf{w}_u$ are the steering vectors for down- and up-going wave fields, respectively.

Inserting Eqs. (14) and (15) into Eq. (13) gives the cross correlation in the frequency domain:

$$C_{ud}(\omega) = d_u(\omega) d_d^H(\omega) = \mathbf{w}_u^H \mathbf{p} \mathbf{p}^H \mathbf{w}_d, \tag{16}$$

where both down- and up-going steering vectors are used.

Using conventional processing the downward steering vector is $\mathbf{w}_d(\omega) = \mathbf{w}(\omega) = [e^{-i\omega s z_1}, e^{-i\omega s z_2}, \ldots]^T$ and the upgoing is $\mathbf{w}_u(\omega) = \mathbf{w}^*(\omega)$. Inserting these expressions into Eq. (13) gives the cross correlation in the frequency domain:

$$C_{ud}(\omega) = \mathbf{w}^T \mathbf{p}\mathbf{p}^H \mathbf{w}. \quad (17)$$

This expression is very similar to the conventional beamformer $\mathbf{w}^H\mathbf{p}\mathbf{p}^H\mathbf{w}$ except that $\mathbf{w}^H$ is replaced with $\mathbf{w}^T$.

As with conventional beamforming[24] there is a spatial aliasing issue which requires the frequency to be less than $c/2d$ (d is element spacing). For broadband methods and a single source, this requirement usually can be relaxed, as aliasing from several angles will average out in the results. However, in the present application the noise comes from all directions and this aliasing component can destroy the response, as illustrated in the next section (Fig. 5).

To reduce spatial aliasing, it is beneficial to apply a depth-dependent shading factor pre-multiplied on the observed pressure vector $\mathbf{p}$. A Kaiser–Bessel window ($\alpha=1.5$) is used here.

D. Averaging

Often the time series is segmented into J time series which are processed separately and then the output is averaged. In that case Eq. (12) will become

$$c_{ud}(t) = \frac{1}{J}\sum_j^J d_{uj}(t) * d_{dj}(-t) = \frac{1}{J}\sum_j^J \int_0^T d_{uj}(\tau) d_{dj}(\tau - t) d\tau, \quad (18)$$

where it is assumed that each time series is sufficiently long that truncation effects can be neglected. In the frequency domain the averaging is efficiently expressed via the estimated cross-spectral density matrix $\mathbf{C}=(1/J)\Sigma_j^J \mathbf{p}_j\mathbf{p}_j^H$. Thus the frequency domain expression becomes

$$C_{ud}(\omega) = \frac{1}{J}\sum_j^J d_{uj}(\omega) d_{dj}^H(\omega) = \mathbf{w}^T\mathbf{C}\mathbf{w}. \quad (19)$$

E. High-resolution adaptive beamforming

The frequency domain response can also be obtained by using high-resolution beamforming methods in Eq. (16) with two adaptive steering vectors. These steering vectors can be obtained using any one of several adaptive processing methods. One possible choice is to use the minimum variance distortionless response with white noise gain constraint (MVDR-WNC) beamformer, see e.g., Ref. 24. Although not explored in this article, we have observed that high-resolution beamforming has a tendency toward giving better resolved reflection sequences in the time domain. An example of this processing is shown in the time series at the right of Fig. 3 in the next section.

F. Frequency band

It is noted from Urick[25] that the ambient noise due to wind decays about 6 dB per octave. Thus, if the frequency spectrum is not normalized the response will be dominated by the lower frequencies. Here, the cross spectral density matrix is normalized by its trace to obtain a flat spectrum. Other normalizations are also possible; for a discussion see Ref. 26.

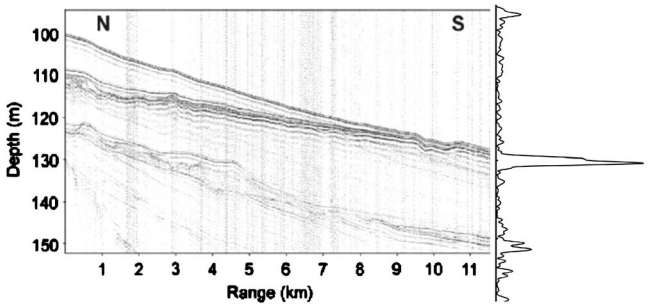

FIG. 3. Seismic section for the Mapex2kbis area (Ref. 29). The location of the vertical array is about 1 km further to the south. To the right the extracted reflection sequence derived from noise, obtained using the MVDR-WNC high resolution adaptive beamformer on the vertical array data.

The minimum and maximum frequency $f_{\min}$ and $f_{\max}$ must be selected for processing. A large bandwidth, i.e., a low $f_{\min}$ and a high $f_{\max}$, is preferable in order to obtain a sharper pulse in the time domain.

The minimum frequency can be selected from the following empirical rules

(1) At low frequencies the noise is dominated by shipping. Urick[25] gives a typical value of 200 Hz as the point where wind noise starts to dominate.
(2) The beam pattern from the end fire beam should be sufficiently narrow that it is not influenced by horizontal propagating noise, which typically propagates with grazing angle of $\pm 30°$ or less. Thus, the lower frequency should be chosen high enough that the width of the end-fire beam is less than $2(90-30)=120°$.

The maximum frequency should be sufficiently low so that the array will not have grating lobes in the horizontal propagating noise direction. Assuming the horizontal propagating noise is within 15° from horizontal then from Eq. (20) a $f_{\max}$ of $2/(1+\sin 15°)f_d = 1.6 f_d$, where $f_d = c/2d$ (array design frequency) corresponds to the frequency where the array elements have spacing $d=\lambda/2$. In practice, it has been found that $f_{\max}=2f_d$ works well.

Finally, in Sec. III A, the depth resolution was found to be $c/2b$ (b is bandwidth and c is sound speed). If b is close to twice the design frequency of the array $b=2f_d=c/d$ then the resolution of the seabed and sediment interface is about $d/2$. Smaller array spacing leads to a higher usable bandwidth and thus better depth resolution.

IV. EXPERIMENT

The data used to demonstrate the approach and its limitations are from the Mapex2kbis experiment on 22 November 2000 (Refs. 27–29), where the vertical array was moored in 130-m deep water with the center of the array at 96-m depth. The site is a sandy bottom in the South Sicily area. The array was nested and two configurations with 32 phones and either 0.5-m spacing or 1-m spacing are used in the analysis.

The experiment took place on the Malta Plateau; for a map of the area see Fig. 1 of Ref. 29. A seismic profile[29] (Fig. 3) was obtained with the array moored 1 km further to

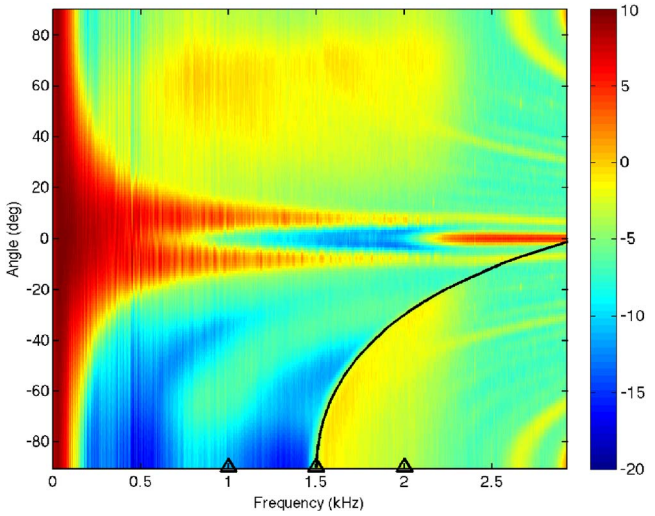

FIG. 4. (Color online) Beamformer output (dB) for the Mapex2kbis data. The grating lobes curve Eq. (20) (solid) is in the lower right corner. This is for a 32-element array with $d=0.5$ m spacing, corresponding to a 1500-Hz design frequency.

the south. For reference, the envelope of the reflection sequence obtained at the array based on the observed ambient noise high-resolution adaptive beamforming (MVDR-WNC) is shown.

For demonstration of the approach, one hundred 10-s samples were used to construct the cross-spectral density matrix. The quality of the estimated time domain Green's functions depends on the observation time. It has been shown[4,6] and observed[14] that the time domain Green's function convergence is proportional to the square root of the observation time. Thus, a much smaller observation time can be used (30 s gives reasonable estimates) at the expense of quality of the estimates. The data were sampled at 6 kHz.[30]

A. Spatial aliasing

In a series of papers Harrison,[27,31,32] demonstrated that bottom properties could be extracted by comparing the down- and up-going energy from a simple beamformer output. The motivation for this approach is that upward propagating ambient noise has one more bottom bounce than downgoing ambient noise at the same angle. Note that this approach is incoherent in the frequency domain whereas the present method is coherent.

An example of the frequency domain conventional beamformer output is shown in Fig. 4 based on the Mapex2kbis data.[27,31] Down-going signals correspond to positive angles and up-going to negative angles. A Kaiser–Bessel window was applied across the phones. The cross-spectral density matrix has been normalized at each frequency by its trace, so that the energy for each frequency is the same (the unnormalized beam response can be seen in Ref. 27). The antialiasing filter begins to roll off at 2 kHz. The nature of the beamformer output changes somewhat around 2.2 kHz, indicating that the compensation for the antialiasing filter also has enhanced data acquisition system self-noise. The nonpropagating electric self-noise can be seen at around 0° at frequencies greater than 2.2 kHz.

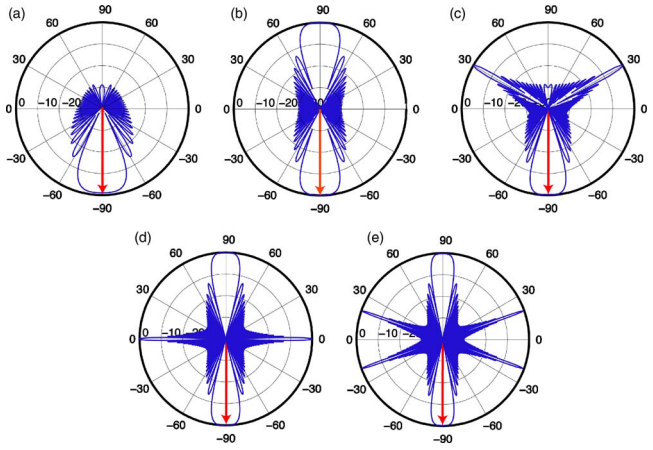

FIG. 5. (Color online) Beam pattern for the downward beam (−90°) at (a) 1 kHz, (b) 1.5 kHz (f_d), (c) 2 kHz ($4/3f_d$), (d) 3 kHz ($2f_d$), and (e) 4.5 kHz ($3f_d$). The first three frequencies used are indicated with △ in Fig. 4. Grating lobes can be seen in (b) at +90°, (c) at +30°, (d) +90°, 0°, and (e) +90°, ±20°.

For frequencies below the design frequency $c/2d$ there is no spatial aliasing, but above this frequency spatial aliasing starts to appear for frequencies and angles larger than the grating angle curve given by[24]

$$f = \frac{c}{d}\frac{1}{1+|\sin\theta|}. \tag{20}$$

This relationship is shown in Fig. 4. Below this curve, the upgoing energy also appears as downgoing energy. This energy from the surface will destroy the ability to extract reflection loss curves,[27] as that processing is based only on magnitude. It may inhibit the ability to extract reflection sequences in the time domain,[10] as this processing is based on both magnitude and phase.

When estimating reflection sequences,[10] one beam is pointing downwards (−90°) and one is pointing upwards (90°). Both of these have similar beam patterns. For the downward beam we explore the variation in beam pattern as the frequency is increased, Fig. 5. Below the design frequency there are no grazing lobes [Fig. 5(a)], but at the design frequency the grazing lobes start to appear [Fig. 5(b)]. As the frequency increases further the grazing lobes appears at lower grazing angles [Figs. 5(c)–5(e)]. The energy that comes in through these grazing lobes can dominate the true response. Thus, the present coherent approach (both phase and magnitude are used) might tolerate minor contributions from the grazing lobes, but the strong energy grazing lobes near horizontal could be a problem.

B. Time response

Reflection sequences were extracted from the noise based on a 0.5-m spacing (Fig. 6) and a 1-m spacing (Fig. 7). The processing is done in the frequency domain. The design frequency f_d is 1500 Hz for the 0.5 m spacing and 750 Hz for 1 m spacing. In the processing the top hydrophone is used as reference depth. The horizontal axis represents depth converted from the two-way traveltime, which is the output of the processing.

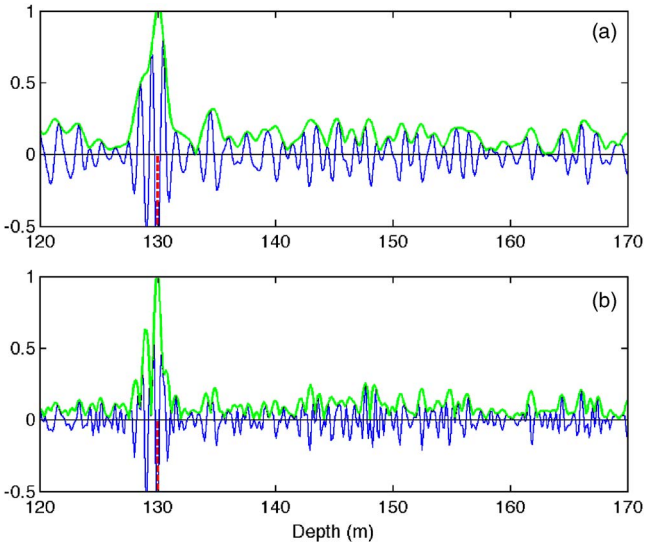

FIG. 6. (Color online) Wave form (thin solid) and envelope (thick solid) impulse response for Mapex2kbis vertical array for 32 phones using 0.5-m spacing and processing in a frequency interval with lower frequency 100 Hz and upper frequency (a) 1500 Hz (f_d) or (b) 3000 Hz ($2f_d$). Bottom is indicated at 130 m depth and a sediment layer can be seen at 145–150 m.

The bottom reflection appears clearly at 130-m depth and the reflection from one or two interfaces at 145–150 m can be seen clearly in Figs. 6 and 7. During the experiment,

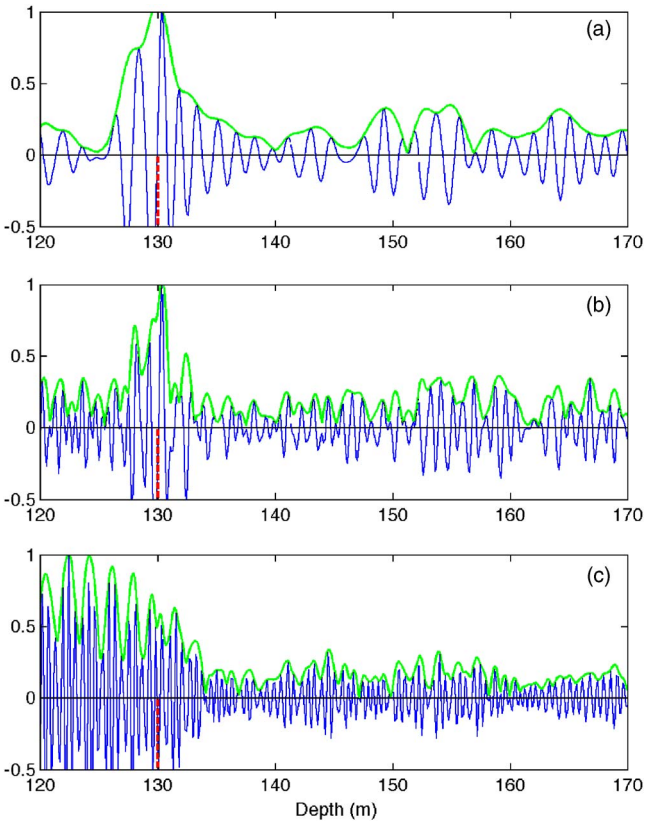

FIG. 7. (Color online) Wave form (thin solid) and envelope impulse (thick solid) response for Mapex2kbis for 32 phones using 1-m spacing and frequency interval (a) 100–750 Hz, (b) 100–1500 Hz, and (c) 100–3000 Hz. With lower frequency 100 Hz and upper frequency (a) 750 Hz (f_d), (b) 1500 Hz ($2f_d$), or (c) 3000 Hz ($3f_d$). Bottom is indicated at 130-m depth and a sediment layer can be seen at 145–150 m.

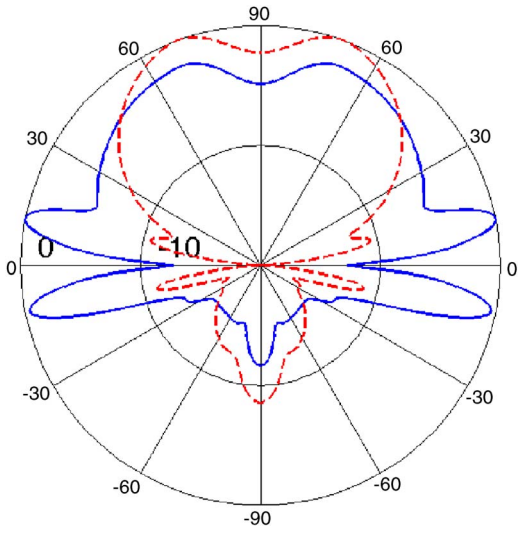

FIG. 8. (Color online) Maximum beampower output (dB) for array of 32 pressure (solid) or vertical velocity sensors (dashed) at frequency 1460 Hz. Each curve is normalized so that the maximum is 0 dB.

a seismic reflection profile was obtained,[29] see Fig. 3. The location of the horizontal array is 1 km south of the southern part of the refection section. The seismic section shows a set of sediment reflectors that are following the ocean bottom at a depth of 15–20 m. This is in clear agreement with the reflectors obtained from the noise processing (Figs. 6 and 7).

The processing was done for several values of the maximum frequency, corresponding to the design frequency f_d [Figs. 6(a) and 7(a)], $2f_d$ [Figs. 6(b) and 7(b)], and $3f_d$ [Fig. 7(c)]. The time series for Figs. 6(b) and 7(b) (corresponding to $2f_d$) seems to give the best resolution indicating that a maximum frequency above the design frequency f_d gives better resolution. The observation for real data is that noise processing gives higher resolution if frequencies above the design frequency are used and about two times the design frequency seems optimal.

V. SIMULATION EXAMPLE

The purpose of the simulations is to further illustrate the processing sensitivity to hydrophone numbers and spacing as well as explore the processing using vertical velocity sensors.[30] Based on the Kuperman–Ingenito model,[19] we simulated the noise field using OASES[33] with the same environment as used in Ref. 10. In the Kuperman–Ingenito model the ocean noise is modeled as a sheet (here at depth 1 m) of spatially and temporally independent sources. This example presents a best case scenario as the simulations assume infinite time averaging.

A geometry similar to the Mapex2kbis experiment is examined: A vertical array with 32 elements with 0.5-m spacing and first element at 84 m. The design frequency is 1500 Hz. The ocean sound speed is constant 1500 m/s. The seabed is at 130 m with layer interfaces at 145 and 150 m depths and bottom sound speed is 1600/1650/1700 m/s and density 1500/2000/2500 kg/m^3 in three bottom layers, respectively.

First, in Fig. 8, we compare the beamformer output at a single frequency (1460 Hz) below the design frequency for

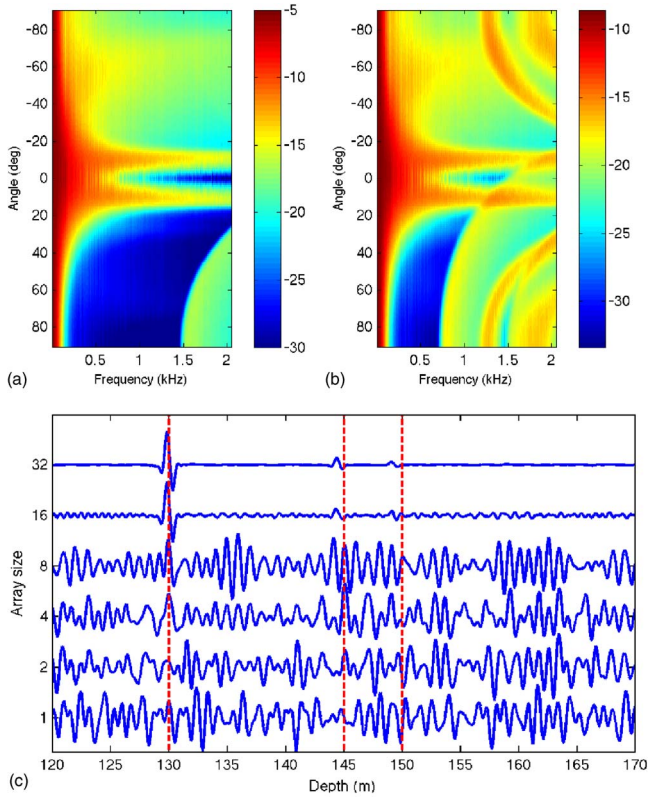

FIG. 9. (Color online) Pressure sensors. Beam response for array with (a) 32 and (b) 16 sensors. (c) Time series for a pressure sensor array. Each trace shows the result of using 32, 16, 8, 4, 2, and 1 sensor, respectively. The array aperture was held constant 15.5 m (except for the 1 sensor). For all signals the time response was computed in the frequency interval 10–1500 Hz and normalized so that the maximum amplitude was one. The interfaces (dashed) are indicated at 130, 145, and 150 m.

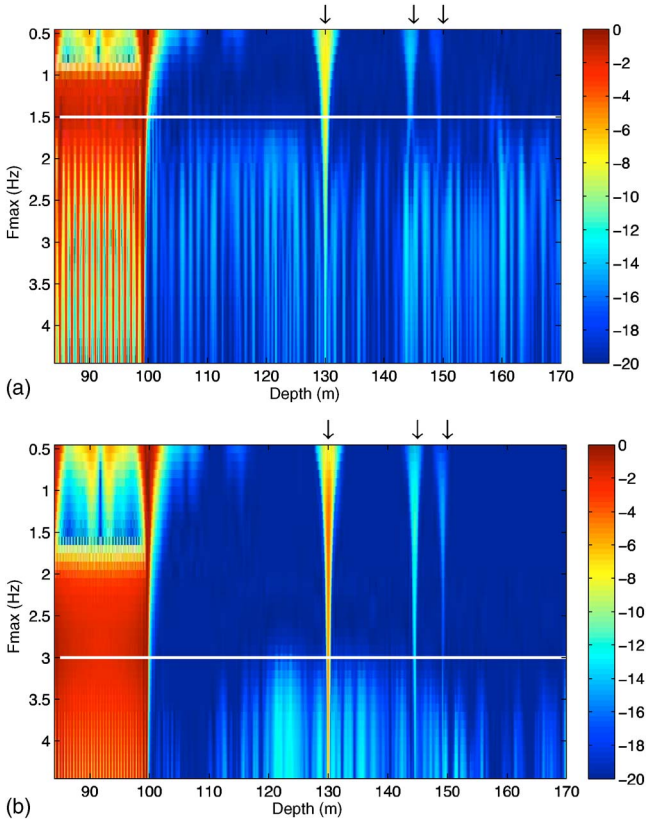

FIG. 10. (Color online) Envelope (dB) of the time response as a function of maximum frequency used for (a) 16 and (b) 32 elements. The minimum frequency was constant 10 Hz and the aperture 15.5 m. Each horizontal line is normalized so that the maximum is 0 dB. The arrows at 130, 145, and 150 m indicates the interfaces. The horizontal white line indicates $2f_d$.

an array consisting of pressure hydrophones (solid) and vertical velocity (dashed) sensors. Due to the waveguide effect there is much more energy in the horizontal direction for the pressure sensors. At higher frequencies, the incoming energy would have a similar pattern, but, due to spatial aliasing (as demonstrated in Fig. 5), this energy appears to come from other directions.

A vertical velocity sensor has a sensor pattern similar to vertical dipole receiver and is thus blind to the horizontal propagating energy. Therefore, the energy is more focused in the vertical direction as shown by the dashed line in Fig. 8. Above the design frequency, the velocity sensor signal would also be aliased, but the effect would be much less, as there is little horizontal signal to be aliased. This reduces the effect of grating lobes away from end-fire.

A. Pressure sensor array

The beam response from the 32 hydrophone array is computed in Fig. 9(a), where the grating lobe is seen starting at the design frequency f_d=1500 Hz. When decreasing the number of phones to 16 (f_d=750 Hz), the aliasing in the beam response, Fig. 9(b), starts appearing at the lower design frequency and it is clear that the beam response is changed below the grating curve that starts at the design frequency. As in the Mapex2kbis data case, Fig. 4, below the grating lobe curve upgoing energy appears as downgoing energy.

The effect on the time domain response of changing the number of phones is investigated in Fig. 9(c). Each of the time series is produced using the same frequency interval 10–1500 Hz (upper band correspond to the design frequency at 1-m spacing). For fixed aperture and fixed upper frequency, when reducing the number of phones the corresponding design frequency reduces by the same factor.

Using all 32 phones (maximum frequency is f_d), the reflections from all three interfaces (130, 145, and 150 m) are seen clearly. (The arrivals for the subbottom bounces [145 and 150 m] appear slightly too early because a constant speed [1500 m/s] instead of the correct sediment speed was used to convert the time axis to depth.) With 16 phones (maximum frequency is $2f_d$), more noise starts appearing on the trace. For fewer phones (maximum frequency is $4f_d$ or more), the subbottom layers cannot be observed and the ocean bottom can barely be observed. The reason for this is that much of the horizontal energy comes in through the sidelobes and this contaminates the calculation of the down- and up-going energy.

The envelope of the time domain response is explored versus the maximum frequency used in the processing for 32 [Fig. 10(a)] and 16 [Fig. 10(b)] elements. First the spurious component can be seen to a depth of 100 m (corresponding to the array length). This tooth-shape response depends on the number of hydrophones, see Sec. II. The reflections from the subbottom start becoming contaminated at a frequency corresponding to $2f_d$ (white horizontal line).

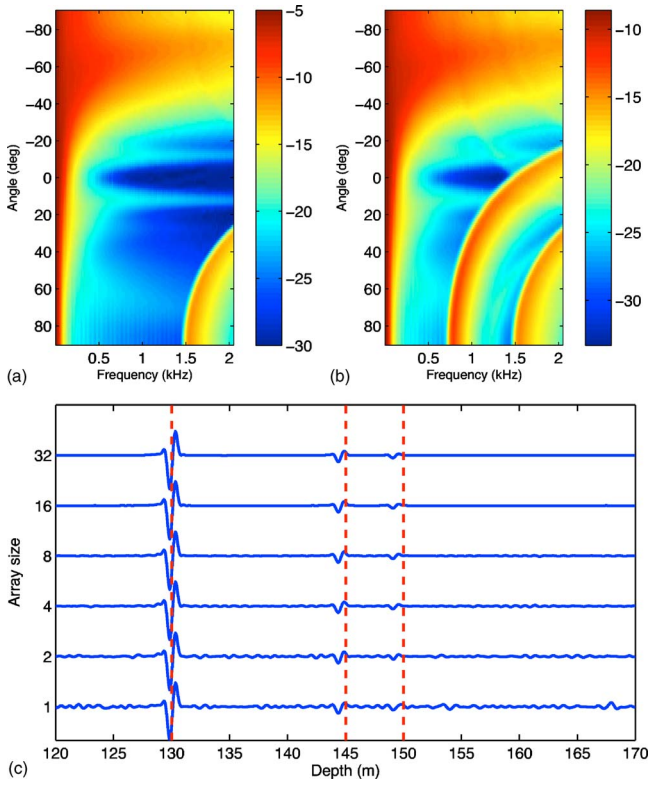

FIG. 11. (Color online) Vertical velocity sensors. Beam response for array with (a) 32 and (b) 16 sensors. (c) Time series for a vertical velocity sensor array. For description see caption in Fig. 9.

B. Vertical velocity sensor array

The same processing as carried out on the hydrophone array (Sec. V A) was carried out with a vertical velocity sensor array, see Fig. 11. As discussed earlier, a vertical velocity sensor is not as sensitive to horizontally propagating energy. This is seen in the beam response in Figs. 11(a) and 11(b).

Figure 11(c) shows the reflection response for the vertical velocity sensors using all 32 phones and then repeating the processing with 16, 8, 4, 2, and 1 phones, similar to the hydrophone array processing (Fig. 9). Note the change in polarity of the wave form relative to the pressure array. It is seen that for a vertical velocity sensor array it is possible to extract the reflection response with just one sensor. The reason being that the vertical velocity sensor is not sensitive to horizontally propagating energy in the waveguide.

VI. CONCLUSION

By array processing of ocean acoustic noise on a vertical array, it is possible to extract the reflection sequence convolved with the noise autocorrelation function. From this, information about the bottom depth and possibly deeper layers can be extracted. A problem in ocean acoustics is that much of the noise is horizontally propagating and this noise dominates the information-carrying vertically propagating noise. Using vertical array processing it is possible to mitigate the impact of the horizontally propagating noise.

When doing noise processing on a vertical array, the reflection response is sensitive to the phone spacing. Generally, the maximum frequency should not be larger that the design frequency of the array. However, higher resolution of the noise reflection sequence often can be obtained with a higher maximum frequency (here about two times the design frequency) and possibly the use of high resolution beamforming techniques.

A way to reduce the spatial sampling requirements is to use a vertical velocity sensor array that rejects horizontally propagating energy. A simulation example indicates that just one vertical velocity sensor is sufficient.

ACKNOWLEDGMENTS

This work was supported by the Office of Naval Research under Grant No. N00014-05-1-0264.

[1]A. Curtis, P. Gerstoft, H. Sato, R. Snieder, and K. Wapenaar, "Seismic interferometry—Turning noise into signal," The Leading Edge **25**, 1082–1092 (2006).
[2]G. D. Bensen, M. H. Ritzwoller, M. P. Barmin, A. L. Levshin, F. Lin, M. P. Moschetti, N. M. Shapiro, and Y. Yang, "Processing seismic ambient noise data to obtain reliable broad-band surface wave dispersion measurements," Geophys. J. Int. **169**, 1239–1260 (2007).
[3]R. L. Weaver and O. I. Lobkis, "Ultrasonics without a source: Thermal fluctuation correlations at MHz frequencies," Phys. Rev. Lett. **87**, 134301 (2001).
[4]R. Snieder, "Extracting the Green's function from the correlation of coda waves: A derivation based on stationary phase," Phys. Rev. E **69**, 046610 (2004).
[5]K. Wapenaar, "Retrieving the elastodynamic Green's function of an arbitrary inhomogeneous medium by cross correlation," Phys. Rev. Lett. **93**, 254301 (2004).
[6]P. Roux, K. G. Sabra, W. A. Kuperman, and A. Roux, "Ambient noise cross-correlation in free space: Theoretical approach," J. Acoust. Soc. Am. **117**, 79–84 (2005).
[7]P. Roux and W. A. Kuperman, "Extracting coherent wave fronts from acoustic ambient noise in the ocean," J. Acoust. Soc. Am. **116**, 1995–2003 (2004).
[8]K. G. Sabra, P. Roux, A. M. Thode, G. L. D'Spain, W. S. Hodgkiss, and W. A. Kuperman, "Using ocean ambient noise for array self-localization and self-synchronization," IEEE J. Ocean. Eng. **30**, 338–347 (2005).
[9]K. G. Sabra, P. Roux, and W. A. Kuperman, "Arrival-time structure of the time-averaged ambient noise cross-correlation function in an oceanic waveguide," J. Acoust. Soc. Am. **117**, 164–174 (2005).
[10]M. Siderius, C. H. Harrison, and M. B. Porter, "A passive fathometer technique for imaging seabed layering using ambient noise," J. Acoust. Soc. Am. **120**, 1315–1323 (2006).
[11]M. Campillo and A. Paul, "Long-range correlations in the diffuse seismic coda," Science **229**, 547–549 (2003).
[12]E. Larose, A. Derode, M. Campillo, and M. Fink, "Imaging from one-bit correlations of wideband diffuse wavefields," J. Appl. Phys. **95**, 8393–8399 (2004).
[13]N. M. Shapiro, M. Campillo, L. Stehly, and M. H. Ritzwoller, "High-resolution surface wave tomography from ambient seismic noise," Science **307**, 1615–1617 (2005).
[14]K. G. Sabra, P. Gerstoft, P. Roux, W. A. Kuperman, and M. C. Fehler, "Extracting time-domain Green's function estimates from ambient seismic noise," Geophys. Res. Lett. **32**, L03310 (2005).
[15]P. Roux, K. G. Sabra, P. Gerstoft, W. A. Kuperman, and M. C. Fehler, "P-waves from cross correlation of seismic noise," Geophys. Res. Lett. **32**, L19303 (2005).
[16]P. Gerstoft, K. G. Sabra, P. Roux, W. A. Kuperman, and M. C. Fehler, "Green's functions extraction and surface-wave tomography from microseisms in southern California," Geophysics **71**, S123–S131 (2006).
[17]K. Wapenaar and J. Fokkema, "Green's function representations for seismic interferometry," Geophysics **71**, SI33–SI46 (2006).
[18]D. Draganov, K. Wapenaar, W. Mulder, J. Singer, and A. Verdel, "Retrieval of reflections from seismic background-noise measurements," Geophys. Res. Lett. **34**, L04305 (2007).
[19]W. A. Kuperman and F. Ingenito, "Spatial correlation of surface generated noise in a stratified ocean," J. Acoust. Soc. Am. **67**, 1988–1996 (1980).

[20]R. Snieder, K. Wapenaar, and K. Larner, "Spurious multiples in seismic interferometry of primaries," Geophysics **71**, SI111–SI124 (2006).
[21]L. A. Brooks and P. Gerstoft, "Ocean acoustic interferometry," J. Acoust. Soc. Am. **121**, 3377–3385 (2007).
[22]K. Mehta, A. Bakulin, J. Sheiman, R. Calvert, and R. Snieder, "Improving the virtual source method by wavefield separation," Geophysics **72**, V79–86 (2007).
[23]A. Papoulis, *Probability, Random Variables and Stochastic Processes* (McGraw-Hill Book Company, New York, 1965).
[24]H. L. Van Trees, *Optimum Array Processing* (Wiley, New York, 2002).
[25]R. J. Urick, *Principles of Underwater Sound* (McGraw-Hill, New York, 1975).
[26]C. H. Harrison and M. T. Siderius, "Bottom profiling by correlating beam-steered noise sequences," J. Acoust. Soc. Am., in press (2008).
[27]C. H. Harrison and D. G. Simons, "Geoacoustic inversion of ambient noise: A simple method," J. Acoust. Soc. Am. **112**, 1377–1389 (2002).
[28]M. Siderius, P. L. Nielsen, and P. Gerstoft, "Range-dependent seabed characterization by inversion of acoustic data from a towed receiver array," J. Acoust. Soc. Am. **112**, 1523–1535 (2002).
[29]M. R. Fallat, P. L. Nielsen, S. E. Dosso, and M. Siderius, "Geoacoustic characterization of a range-dependent ocean environment using towed array data," IEEE J. Ocean. Eng. **30**, 198–206 (2005).
[30]P. Hursky, "Modeling and processing for vector sensors," Office of Naval Research, Ocean Acoustics Annual Report 2006 (also available at http://www.onr.navy.mil/obs/reports/docs/06/oahursky.pdf, last visited 20 September 2007).
[31]C. H. Harrison, "Sub-bottom profiling using ocean ambient noise," J. Acoust. Soc. Am. **115**, 1505–1515 (2004).
[32]C. H. Harrison, "Performance and limitations of spectral factorization for ambient noise sub-bottom profiling," J. Acoust. Soc. Am. **118**, 2913–2923 (2005).
[33]H. Schmidt, *OASES Version 3.1 User Guide and Reference Manual* (MIT, Cambridge, 2004).